Coupling strength distribution in ferromagnetic/antiferromagnetic film systems

K. Steenbeck and R. Mattheis
Institute of Photonic Technology, Albert Einstein Strasse 9, D-07745 Jena, Germany
(Received 7 September 2006; revised manuscript received 15 February 2007; published 23 April 2007)

Exchange coupling of a polycrystalline ferromagnetic(F)/antiferromagnetic(AF) film system is the superposed action of grains each with an individual coupling strength j represented by a probability function $P(j)$. $P(j)$ governs the entire film coupling and the exchange bias field, and was not measurable until now. We propose a method to determine $P(j)$ from the high field rotational energy losses at low temperatures of a film system with low thickness of the AF layer. The method is verified by torquemetry in a rotating field after reversing its rotational sense. The transition to a new magnetic steady state after the reversal is analyzed within a Stoner-Wohlfarth model including thermal relaxation. This transition is completed earlier for strongly coupled grains than for grains with smaller j, which is reflected in the angular dependence of the hysteretic torque. We determined $P(j)$ for a sputtered NiFe(16 nm)/IrMn(0.8 nm) film at $T=10$ K and 50 K in the hysteretic range of coupling energies and found that P decreases with increasing j.

DOI: 10.1103/PhysRevB.75.134419 PACS number(s): 75.50.Ee, 75.30.Et, 75.70.Cn

I. INTRODUCTION

The interaction at the interface between an antiferromagnet (AF) and a ferromagnet (F) establishes a unidirectional magnetic anisotropy and a shifted hysteresis loop, which is very useful for the definition of a reference direction in magnetoelectronic devices. This so-called exchange bias (EB) effect was discovered a long time ago by Miklejohn and Bean,[1] and has found wide application in the last 10 years. A detailed understanding, however, is not possible until now due to the random nature of the EB. A coupled F/AF film always consists of local different regions (grains, domains,…) with their individual couplings j to the F magnetization.[2–4] Assuming constant AF anisotropy, then regions with low coupling cause the EB, while regions with medium coupling induce rotational loss and increased coercivity, and regions with high coupling do not contribute to any of these phenomena. Therefore, the observable properties depend on the distribution of the coupling energies, which is characterized by a coupling strength distribution function $P(j)$ independent of the nature of the local subdivision. $P(j)dj$ is the portion of grains with a coupling strength between j and $(j+dj)$. Different models have been applied to explain j and $P(j)$ which consider the AF net moment, F magnetization, exchange constant, grain size, grain size distribution, interface roughness, etc. Comprehensive explanations about the mechanisms in polycrystalline F/AF systems are given in Refs. 3 and 5–10. Systems with AF films of very small thickness t behave like ensembles of noninteracting grains with a homogeneous magnetization M_{AF} coupled to the F layer.[11,12] The interactions can be neglected due to the small intergrain contact area and M_{AF} is homogeneous within each grain as long as t is small compared to the AF domain wall thickness.[13] To the best of our knowledge, the distribution $P(j)$ was not measurable until now, but has merely been adapted from a theoretical understanding with statistical assumptions.[3,14,12,15] Much experimental work was reported on the distribution of blocking temperatures and of relaxation times in different F/AF film systems.[16,17,10,18,19,9] They give an idea about the distribution of energy barriers, for example due to different grain sizes,[10] or anisotropy constants,[9] but a distribution of coupling strength has not been verified experimentally.

In order to overcome this situation, we analyze the transition from the steady state of a F/AF film system in a rotating magnetic field to a new steady state after reversal of the field's rotational direction. For each grain this transition depends on its F/AF coupling strength j. Strongly coupled grains gain their new equilibrium state earlier than grains of the same anisotropy but with weak coupling j. We analyzed this transition behavior by torque magnetometry at a low temperature T and a high magnetic field for (111) textured NiFe/IrMn films with a low thickness $t \leqslant 2$ nm of the IrMn and a thickness $t_F=16$ nm of NiFe. By studying the hysteretic behavior we developed a method to determine the exchange coupling strength distribution $P(j)$ based on a Stoner-Wohlfarth-model which includes thermal relaxation effects. This method gives $P(j)$ in the hysteretic range of coupling energies. For a (111) textured film at zero temperature $(T=0)$ this range is $j=(3$ to $18)$ Kt, where K is the AF anisotropy energy density which in this case has a 3-axial symmetry. By means of the experimental results advantages and limits of the measuring method are discussed.

II. MODEL FOR TEMPERATURE $T=0$

A. Hysteretic torque curves in rotating fields

The F film of F/AF film combinations in fields $H \geqslant 400$ kA/m is magnetically saturated. Therefore, all contributions to the torque hysteresis result from the AF and its coupling to the F. We use a model for polycrystalline textured F/AF film systems with very low AF thickness similar to the models proposed by Tsunoda[5] and discussed by Fujiwara.[3] We take a q-axial AF anisotropy in the film plane, especially $q=3$ which is adapted to (111) textured films. As a first step in this section we neglect thermal effects. In more detail our assumptions are:

(a) uniform magnetization M_F of the F film,

(b) textured film with the texture axis perpendicular to the film plane and with two-dimensional (2D) randomly distributed AF grains,

(c) all grains with the same values of thickness t, volume v and anisotropy K,

(d) q axial in plane AF anisotropy energy K per volume,

(e) thickness of the AF film $t \leqslant 2$ nm, continuous structure without pinholes,

(f) uniform AF magnetization M_{AF} of a grain (neglecting domain walls, fanning and spin-flop coupling),

(g) coupling with the energy j per area of a grain net moment μ of noncompensated AF interface spins to M_F and rigid coupling between μ and M_{AF} for all grains,

(h) no interaction between AF grains,

(i) M_F and μ lying in the film plane,

(j) temperature $T=0$.

First we consider a single F/AF coupled grain. Applying the Stoner-Wohlfarth-model we use the following expression for the energy e per area

$$e = Kt \sin^2(q\alpha) - j \cos(\beta - \alpha). \tag{1}$$

With respect to an AF easy axis β is the direction of the F layer magnetization M_F (which in the large applied fields practically coincides with the field direction β_H) and $\alpha=\alpha(\beta)$ is the direction of the AF interface net moment μ. Terms for F anisotropies are neglected in Eq. (1), because they do not contribute to the hysteresis. In Fig. 1 is illustrated (a) the vector diagram for a 3-axial anisotropy, (b) the function $\alpha(\beta)$ calculated for different coupling j/Kt, and (c) the energy loss $\Delta e/Kt$ for a 360° field rotation (six switching processes) calculated as a function of j/Kt. The function $\alpha(\beta)$ has jumps at certain angles β_s if the coupling energy is in a distinct region $j_1 < j < j_2$. This is connected with rotational energy losses $\Delta e(j)$ due to steplike rotation of the whole spin system in the AF. For $j < j_1$ the AF net moment μ cannot change its direction from one easy axis to the next one thus unidirectional anisotropy and the EB appear and $\Delta e=0$. The critical coupling values for $T=0$ are $j_1=qKt$ and $j_2=2qj_1$. With the conditions $\delta e/\delta\alpha=0$ and $\delta^2 e/\delta\alpha^2 > 0$ we get the torque L normalized to Kv

$$-\frac{L}{Kv} = \frac{1}{Kt}\frac{de}{d\beta} = f(\beta). \tag{2}$$

Figure 2 shows calculated torque curves $f(\beta)$ for a single (111) oriented grain ($q=3$) for clockwise (cw) and counterclockwise (ccw) field rotation over several periods and after a rotation reversal. Figure 2(a) is for small and 2(b) for larger coupling. Starting the field rotation with increasing β (clockwise, cw) from point A in Fig. 2(a) which corresponds to ($\beta=0$; $\alpha=0$) $f(\beta)$ reaches at point B a periodic function $f_{cw\text{-}p}(\beta)$ (dark line). At the switching angle β_s (point C) $f(\beta)$ jumps to point D with the lower value $f(\beta_s - 60°)$. The function $f_{cw\text{-}p}(\beta)$ has a sawtoothlike shape with the period $\beta_p=\pi/q=60°$ and switches at the angles $\beta_{scw}=\beta_s+n\ 60°$, ($n=0;\pm1;\pm2;\ldots$). After reversal to counterclockwise (ccw) rotation, for example at point E, $f(\beta)$ follows the transition function $f_{ccw\text{-}t}$ and reaches after a ccw rotation by an angle Φ_e the corresponding point E' on the periodic function $f_{ccw\text{-}p}(\beta)$ (grey line) which switches at the angles $\beta_{sccw}=-\beta_s+m\ 60°$, ($m=0;\pm1;\pm2;\ldots$). The angle β_s depends on the coupling parameter j/Kt (Fig. 3) and was calculated with Eq. (1) by applying the conditions

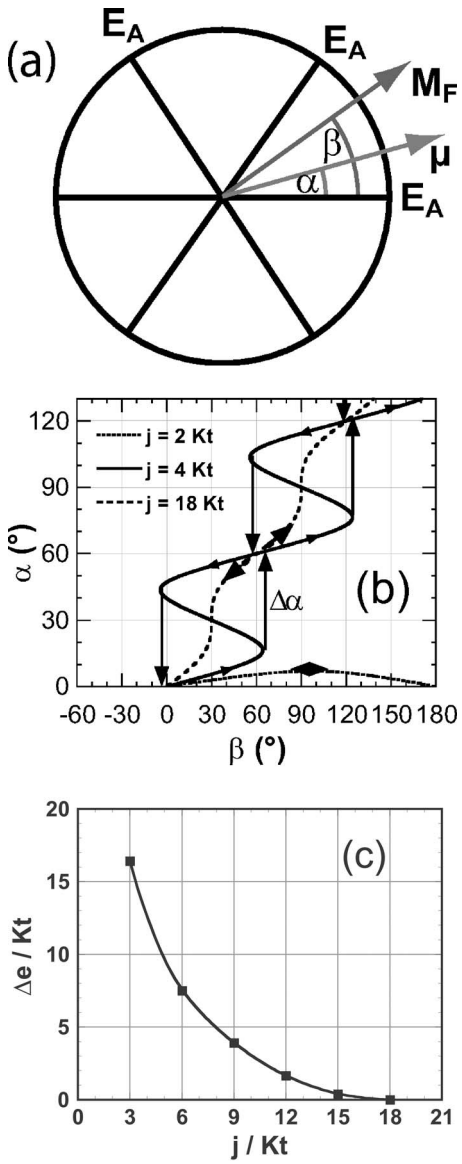

FIG. 1. Model for 3-axial AF anisotropy: (a) AF net moment μ coupled to the easy axes E_A of the AF and to the F magnetization M_F. (b) Direction α of the moment μ dependence on the F magnetization direction β. (c) Energy loss Δe for a 360° field rotation dependence on the coupling energy density j (both normalized).

$$\delta e/\delta\alpha = 0 \text{ and } \delta\beta/\delta\alpha = 0. \tag{3}$$

The angle Φ_e equals the difference between the angles at D and D' and is given by

$$\Phi_e = 2\beta_s - \beta_p. \tag{4}$$

As shown in Fig. 3 Φ_e is small for strong coupling and maximum for weak coupling at $j=j_1$. The maximum Φ_e is equal to 150° for the 3-axial anisotropy ($q=3$), but it is (135°; 90°) for $q=(2;1)$. The maximum f equals $f_{max}=q$ because the torque can never surpass the contribution $Kvq \sin(2q\alpha)$ from the AF anisotropy.

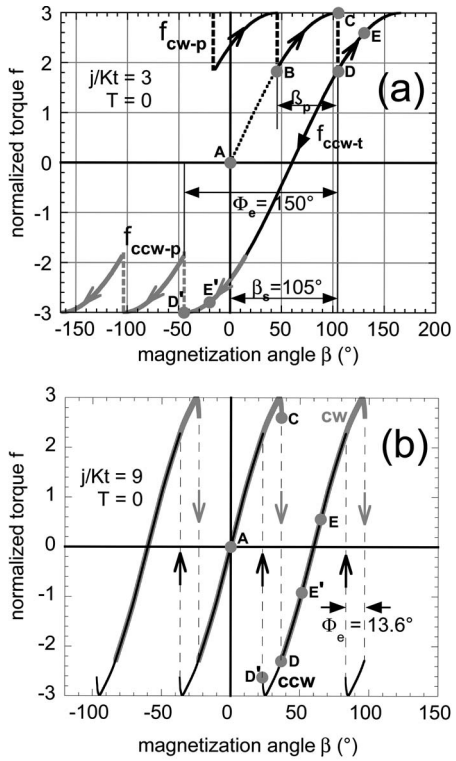

FIG. 2. Normalized torque $f=-L/Kv$ as a function of the ferromagnetic magnetization direction β calculated with Eq. (2) for a (111) oriented grain with (a) weak coupling $j/Kt=3$ and (b) strong coupling $j/Kt=9$. The markings mean: cw=clockwise, ccw=counterclockwise, β_s=switching angle, β_p=period angle, and Φ_e=equilibrium angle.

Now we consider a polycrystalline textured film with grains of the same coupling j but oriented with a random distribution around the field rotation axis. In this case the mean normalized torque $\bar{f}$ of a grain is the average over the contributions $f(\beta_i)$ of all grain orientations where β_i is the magnetization direction of M_F for the grain i. For cw rotation the mean value of the periodic function $f_{cw\text{-}p}$ is a constant

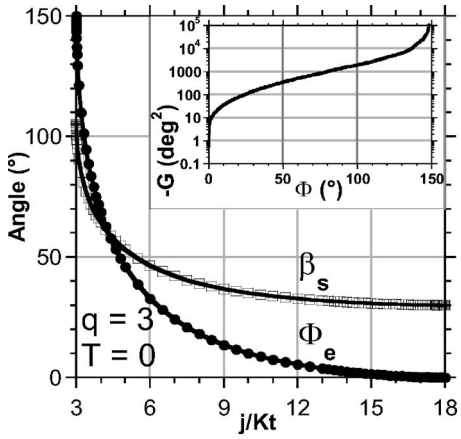

FIG. 3. Switching angle β_s and equilibrium angle Φ_e as a function of the normalized coupling energy j/Kt calculated for a 3-axial anisotropy K. Inset: Calculated function $G(\Phi)$ used in Eq. (17).

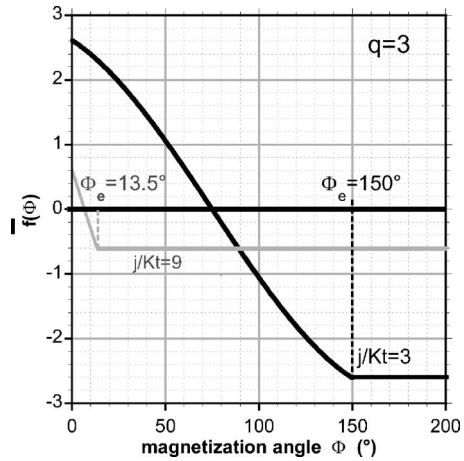

FIG. 4. Mean torque $\bar{f}(\Phi)$ of a single grain calculated for a (111) textured film with constant coupling j/Kt as a function of the magnetization direction Φ after rotation reversal.

$$\bar{f}_{cw\text{-}p} = \frac{1}{\beta_p}\int_{\beta-\beta_p}^{\beta} f_{cw\text{-}p}(\beta_i)d\beta_i. \tag{5}$$

$\bar{f}_{cw\text{-}p}$ is independent of β and it is maximum for $j=j_1$. However, $\bar{f}_{cw\text{-}p}$ reduces for increasing j and vanishes at j_2 where the torque curves become nonhysteretic. After a rotation reversal to the ccw direction each grain changes its torque contribution from $f(\beta_i)$ to $f(\beta_i\text{-}\Phi)$, where Φ is the direction of M_F after rotation reversal, starting with $\Phi=0$ at the reversal point and increasing with ccw rotation. Again, the mean torque of a grain after rotation reversal is independent of β but it depends on Φ because after reversal f follows a transition function $f_{ccw\text{-}t}$ corresponding to that in Fig. 2(a). At $\Phi=0$ the mean value $\bar{f}(\Phi)$ equals $\bar{f}_{cw\text{-}p}$, then it decreases with increasing Φ and after ccw rotation by Φ_e it obtains the new equilibrium value $\bar{f}(\Phi_e)=\bar{f}_{ccw\text{-}p}=-\bar{f}(\Phi=0)$. Again, for $\Phi \geqslant \Phi_e$, $\bar{f}(\Phi)$ remains constant

$$\bar{f}(\Phi) = \frac{1}{\beta_p}\int_{\beta_i=\beta-\beta_p}^{\beta} f_{ccw\text{-}t}(\beta_i-\Phi)d\beta_i$$
$$= \frac{1}{\beta_p}\int_{\beta_S-\Phi-\beta_p}^{\beta_S-\Phi} f_{ccw\text{-}t}(\beta_i)d\beta_i. \tag{6}$$

Figure 4 shows $\bar{f}(\Phi)$ calculated for weak coupling $j/Kt=3$ and strong coupling $j/Kt=9$.

In a real polycrystalline textured F/AF film system we have a distribution $P(j)$ of all possible coupling energy densities, with $\int_0^\infty P(j)dj=1$, and different torque functions $f(\beta,j)$. The portion $P(j)dj$ of all grains in a film with the volume V has the coupling j and contributes with $KVP(j)\bar{f}(j)dj$ to the hysteretic torque of the whole film.

Upon reversing the field direction from cw to ccw there are different equilibrium angles $0 \leqslant \Phi_e(j) \leqslant 150°$ and the torque $L(\Phi)$ for the film is

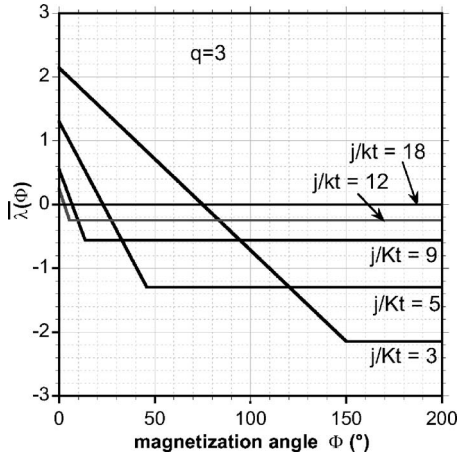

FIG. 5. Approximated mean torque $\bar{\lambda}(j,\Phi)$ of a single grain [corresponding to Eq. (11) and used for $P(j)$ calculation] for the various coupling j/Kt as a function of the magnetization direction Φ.

$$-L(\Phi) = KV\int_{j_1}^{j_2} P(j)\bar{f}(j,\Phi)dj, \tag{7}$$

where $\bar{f}(j,\Phi)$ is taken from Eq. (6) with $f_{\text{ccw-}t}(\beta_i) = f_{\text{ccw-}t}(j,\beta_i)$

$$\bar{f}(j,\Phi) = \begin{cases} \dfrac{1}{\beta_p}\displaystyle\int_{\beta_s(j)-\beta_p-\Phi}^{\beta_s(j)-\Phi} f_{\text{ccw-}t}(j,\beta_i)d\beta_i & \text{for } \Phi < \Phi_e(j) \\ -\bar{f}(j,0) & \text{for } \Phi \geqslant \Phi_e(j). \end{cases} \tag{8}$$

For an easier calculation of the distribution function $P(j)$ we approximate $f_{\text{ccw-}t}(j,\beta)$ by a linear dependence $\lambda(j,\beta)$ with unchanged β_s, β_p, and maximum q

$$f_{\text{ccw-}t}(j,\beta) \approx \lambda(j,\beta) = q\beta/\beta_s(j). \tag{9}$$

Thus the integral in Eq. (8) can be evaluated and we get

$$-L(\Phi) = KV\int_{j_1}^{j_2} P(j)\bar{\lambda}(j,\Phi)dj, \quad \text{with} \tag{10}$$

$$\bar{\lambda}(j,\Phi) = \begin{cases} -q\dfrac{2\Phi - \Phi_e(j)}{\Phi_e(j)+\beta_p} & \text{for } \Phi < \Phi_e(j) \\ -q\dfrac{\Phi_e(j)}{\Phi_e(j)+\beta_p} & \text{for } \Phi \geqslant \Phi_e(j). \end{cases} \tag{11}$$

Figure 5 shows $\bar{\lambda}(j,\Phi)$ as a function of Φ, exemplary for $j/Kt = 3$ (5; 9; 12; 18). By comparison with Fig. 4 we can see that $\bar{\lambda}(j,\Phi)$ is an acceptable approximation of $\bar{f}(j,\Phi)$.

With given functions of $P(j)$ we can calculate the associated torque curves $L(\Phi)$ by applying Eq. (10). Figure 6 shows such curves, normalized to their initial values $L(\Phi=0)$. Their different shapes reflect the different distribution functions which are $P(j)=\text{const}$ (curve c) and the Delta-functional distributions $P(j)=\delta(3Kt)$ (curve a) and $P(j)=\delta(10Kt)$ (curve b). For comparison, a measured curve

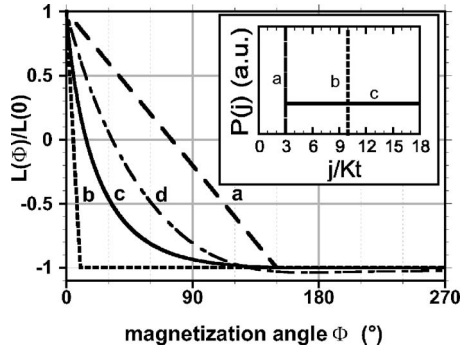

FIG. 6. Torque L (normalized) after magnetic field rotation reversal as a function of the ferromagnetic magnetization direction Φ. Curves a, b, c are calculated for the corresponding coupling distributions $P(j/Kt)$ shown in the inset, and d is an experimental curve for an IrMn film of thickness $t=0.8$ nm.

(d) for a NiFe/IrMn film of thickness $t=0.8$ nm (see paragraph 4) is shown.

As already mentioned in the introduction observable film properties like the exchange bias field H_{EB} and an enhancement ΔH_C of the coercivity H_C are linked with the coupling strength distribution $P(j)$

$$H_{\text{EB}} = (c/M_F t_F)\int_0^{j_1} P(j)jdj. \tag{12}$$

Here $c<1$ is a factor not described in detail here which depends on the film texture and the degree of preferred moment orientation after field cooling.

The total energy loss density E_L per turn is given by

$$E_L = \int_{j_1}^{j_2} P(j)\Delta e(j)dj. \tag{13}$$

It is obtained from the maximum difference between the cw and the ccw torque curve, $E_L=(\pi/S)\Delta L(\Phi=0)$. Due to E_L the coercivity is enhanced by

$$\Delta H_C \propto \int_{j_1}^{j_2} P(j)\Delta e(j)dj. \tag{14}$$

B. Determination of coupling strength distribution

In order to determine $P(j)$ from experimental torque curves $L(\Phi)$ we need the first and second derivative of Eq. (10)

$$-\frac{1}{KV}\frac{dL}{d\Phi} = \int_{j_1}^{j_2} P(j)\frac{\partial\bar{\lambda}(j,\Phi)dj}{\partial\Phi} = \int_{j_1}^{j_{e(\Phi)}} P(j)\frac{\partial\bar{\lambda}}{\partial\Phi}dj + \int_{j_{e(\Phi)}}^{j_2} P(j)\frac{\partial\bar{\lambda}}{\partial\Phi}dj, \tag{15}$$

Where $j_e(\Phi)=j(\Phi=\Phi_e)$. The second term of Eq. (15) is zero due to Eq. (11). Therefore, we can calculate the curvature of the torque curve $L(\Phi)$, noting that both the integrand and the integration limit depend on Φ

$$-\frac{1}{KV}\frac{d^2L}{d\Phi^2}=\frac{d}{d\Phi}\int_{j_1}^{j_e(\Phi)}P(j)\frac{\partial\bar{\lambda}(j,\Phi)}{\partial\Phi}dj$$

$$=\int_{j_1}^{j_e(\Phi)}P(j)\frac{\partial^2\bar{\lambda}}{\partial\Phi^2}dj+P(j_e)\left.\frac{\partial\bar{\lambda}(\Phi)}{\partial\Phi}\right|_{\Phi_e}\frac{dj_e}{d\Phi}. \tag{16}$$

Due to Eq. (11), the first term in Eq. (16) is zero. With

$$\left.\frac{\partial\bar{\lambda}(\Phi)}{\partial\Phi}\right|_{\Phi_e}=-\frac{q}{\beta_s} \tag{16a}$$

and

$$\frac{dj_e}{d\Phi}=\frac{dj}{d\Phi_e}=Kt\frac{d(j/Kt)}{d\Phi_e}, \tag{16b}$$

we get

$$P(j_e)=\frac{1}{KV}\frac{d^2L}{d\Phi^2}\frac{1}{Kt}\frac{d\Phi_e}{d(j/Kt)}\frac{\beta_s}{q}. \tag{16c}$$

Thus

$$P(j)=P[j_e(\Phi)]=\frac{G(\Phi)}{(Kt)^2S}\frac{d^2L(\Phi)}{d\Phi^2}, \tag{17}$$

with the calculable function $G(\Phi)$

$$G(\Phi)=\left[\frac{d\Phi_e/d(j/Kt)}{q/\beta_s}\right]_{\Phi=\Phi_e}. \tag{18}$$

For the calculations of $G(\Phi)$ we use $\Phi_e(j/Kt)$ from Fig. 3 and $q/\beta_s=6/(\Phi+60°)$. $G(\Phi)$ is plotted in the inset of Fig. 3. $S=V/t$ is the film area. Equation (17) gives $P(j)$ at a position Φ of the measured $L(\Phi)$ curve which corresponds to the coupling j/Kt, where this is determined from $\Phi=\Phi_e(j/Kt)$ in Fig. 3.

At $T=0$, Eq. (17) can also be applied to film systems with grains of different products Kt. In this case Eq. (17) on the right gives the distribution function $P(j/Kt)$ of grains with the same ratio j/Kt.

Equation (17) has been verified by its application to a simulated torque curve $L(\Phi)$ consisting of 65 points created with a constant value $P=4/Kt$ in the whole range $j/Kt=3$ to 18. After a polynomial curve fit of these points with $L(\Phi)/KV=A_0+A_1\Phi+A_2\Phi^2+\cdots+A_{10}\Phi^{10}$ and by applying its second derivative, $P=4/Kt\pm5\%$ was reproduced for nearly the whole range $\Phi=1$ to 140°.

III. MODEL FOR $T>0$

In this section we extend the model described in Sec. II by including the influence of thermal energy on the switching process of the AF net moment. With a thermal energy k_BT this switching from an angle α_1 to α_2 takes place for a smaller magnetization angle $\beta<\beta_s(T=0)$ because an energy barrier E_B between the two states can be overcome within a relaxation time $\tau\approx10^{-9}$ s $\exp(E_B/k_BT)$. For $\tau=1$ s, which is comparable with the measuring time at field rotation, the ratio of thermal energy to the barrier must be $k_BT/E_B=1/\ln 10^9$. Figure 7 shows exemplary the normalized energy density e/Kt of a single grain with $j/Kt=3.1$ as a function of α for the magnetization angles $\beta=91°$ and $\beta=60°$ according to Eq. (1).

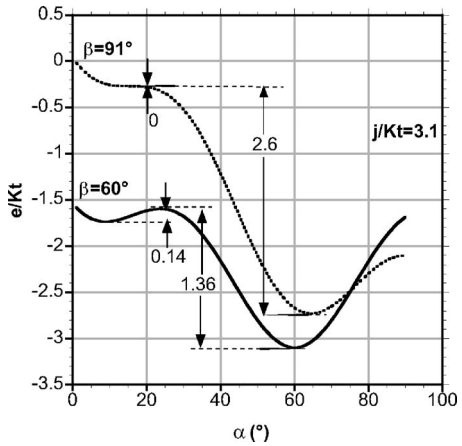

FIG. 7. Normalized energy density e/Kt of a single grain with coupling $j/Kt=3.1$ as a function of the AF moment direction α for constant F magnetization directions β. Dotted curve: $\beta=91°=\beta_s(T=0)$. Solid curve: $\beta=60°=\beta_s(k_BT/Kv=0.0068)$.

The angle $\beta=91°=\beta_s(T=0)$ is the switching angle at $T=0$ because the energy barrier is zero. The energy loss for a full magnetization rotation (six jumps) is given by $\Delta e/Kt=6\times2.6=15.6$. However, for $\beta=60°$ there is a normalized barrier $e_B/Kt=0.14$ which needs a thermal energy $k_BT=(e_B/Kt)^*Kv/\ln 10^9=0.0068\,Kv$ in order to be overcome. This means that $\beta=60°$ is the switching angle β_s for a thermal activation with $k_BT/Kv=0.0068$. (This activation corresponds to a temperature $T=21$ K for $v=(\pi/4)\times(15\text{nm})^2$ 0.8 nm and $K=3\times10^5$ J/m^3.) The normalized energy loss for this case is much smaller and given by $\Delta e/Kt=6\times1.36=8.2$.

Similarly we calculated for different temperatures and anisotropy constants the angles β_s [Fig. 8(a)], Φ_e [Fig. 8(b)] and the energy loss $\Delta e/Kt$ [Fig. 8(c)] as a function of the coupling j/Kt. The parameter in these plots is the ratio k_BT/Kv of thermal energy and anisotropy energy of a grain. Therefore, doubling the measuring temperature changes the switching behavior in the same way as does reducing the anisotropy constant by a factor 1/2 or the crystallite diameter by a factor $1/\sqrt{2}$.

At $T>0$ additional grains with $j/Kt<q$ contribute to the torque hysteresis. The coupling range for switching $j_1<j<j_2$ is shifted to lower values for $T>0$ and for smaller K. The range of switching angles, however, $30°<\beta_s<105°$ and $0<\Phi_e<150°$, remains unchanged because they are determined only by the symmetry of the anisotropy $q=3$. Furthermore, due to the lowered j_1 at $T>0$ the unidirectional anisotropy and the exchange bias field H_{EB} are reduced which is not considered in detail here. The energy loss $\Delta e/Kt$ strongly decreases with increasing temperature as can be seen in Fig. 8(c).

Figure 9 shows calculated torque curves $f(\beta)$ including thermal activation exemplary for $j/Kt=3.0$ and 2.2. Only the

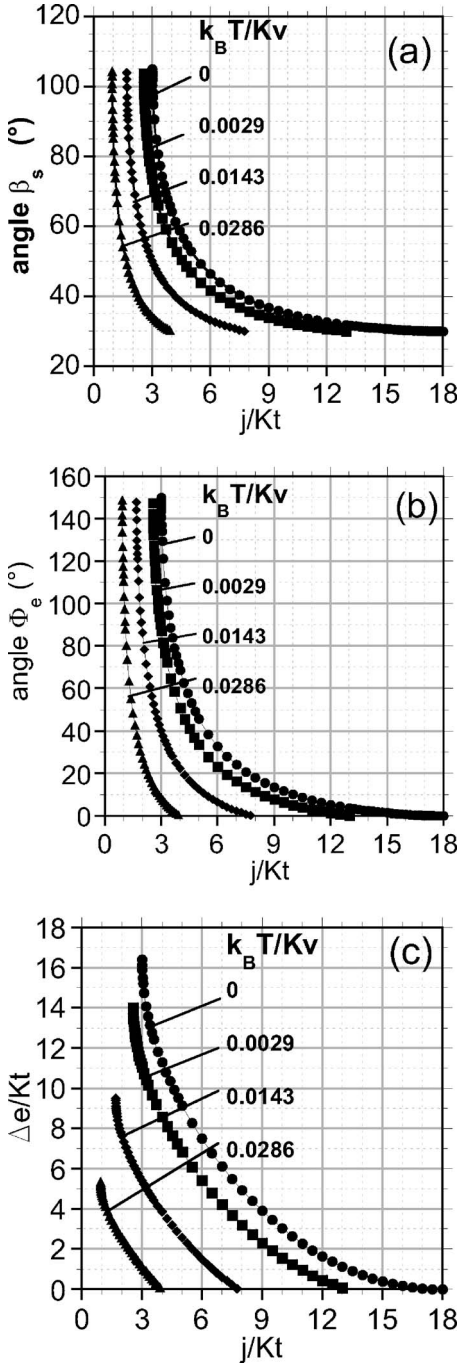

FIG. 8. Critical field angles and energy loss of a single grain as a function of coupling j/Kt for different thermal activation k_BT/Kv. (a) switching angle β_s, (b) equilibrium angle Φ_e, and (c) energy loss $\Delta e/Kt$.

torque for clockwise field rotation is plotted. As compared with $T=0$, for $j/Kt=3.0$ the maximum torque is reduced from $f_{\max}=q=3$ to 2.4 due to the reduction of the switching angle β_s from 105° to 62°. For $j/Kt=2.2$, however, $f_{\max}=2.2$ and $\beta_s=96°$.

When considering a polycrystalline textured film at $T>0$ Eqs. (5)–(8) in Sec. II are still valid provided that the T-specific angles $\beta_s(T)$ and the appropriate torque functions $f[\beta,j,\beta_s(T)]$ are applied. However, for $j/Kt<q$, the approximated linear function $\lambda(j,\beta)$ in Eq. (9) has to be modified because $f_{\max}(T=0)$ is changed from q to j/Kt. We take

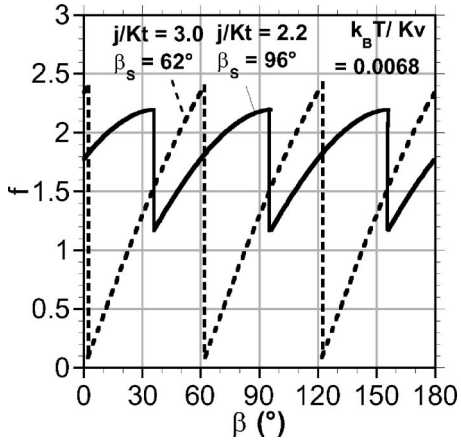

FIG. 9. Normalized torque $f=-L/Kv$ as a function of increasing ferromagnetic magnetization angle β (cw curve) calculated for a single grain with thermal activation $k_BT/Kv=0.0068$ and with coupling $j/Kt=3$ and 2.2.

$$f(j,\beta)\approx\lambda(j,\beta)=\beta^*q/\beta_s(j,T=0)\quad\text{for } j/Kt\geqslant q, \tag{9a}$$

$$f(j,\beta)\approx\lambda(j,\beta)=\beta^*(j/Kt)/\beta_s(j=3Kt)$$
$$=\beta^*(j/Kt)/105\,^\circ\quad\text{for } j/Kt<q. \tag{9b}$$

The coupling strength distribution $P(j)$, analogical to Eq. (17), can be determined from the measured torque curve $L(\Phi,T)$ and the functions $G(\Phi,T)$ and $\Phi=\Phi_e(j/Kt,T)$ which both must be selected with regard to the activation parameter k_BT/Kv

$$P(j)=P[j_e(\Phi,T)]=\frac{G(\Phi,T)}{(Kt)^2S}\frac{d^2L(\Phi,T)}{d\Phi^2}, \tag{17a}$$

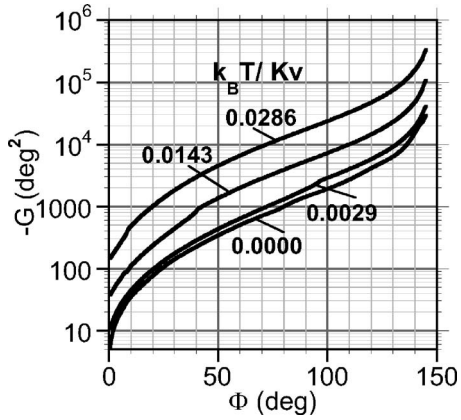

FIG. 10. Function $G(\Phi)$ calculated with Eqs. (18a) and (18b) from the switching angle $\Phi_e(j/Kt)$ of a single AF grain for different thermal activation k_BT/Kv. The kinks in the curves correspond to the changed approximation in Eqs. (9a) and (9b) at $j/Kt=3$.

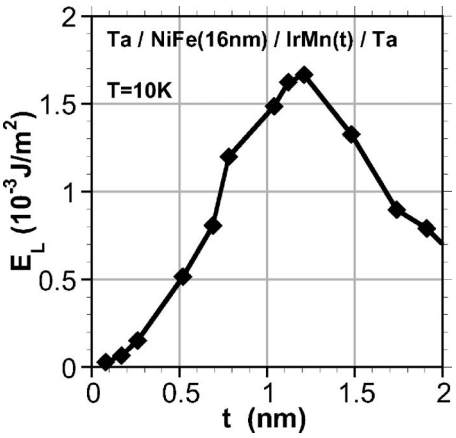

FIG. 11. Energy loss density E_L per turn and per area in the equilibrium state of field rotation as measured for film systems of different IrMn thickness t. $E_L=(\pi/S)\Delta L(\Phi=0)$.

$$G(\Phi,T)=\left[\frac{d\Phi_e(T)/d(j/Kt)}{q/\beta_s(j,T=0)}\right]_{\Phi=\Phi_e(T)} \quad \text{for } j/Kt \geqslant q. \tag{18a}$$

$$G(\Phi,T)=\left[\frac{d\Phi_e(T)/d(j/Kt)}{j/Kt * 105^\circ}\right]_{\Phi=\Phi_e(T)} \quad \text{for } j/Kt < q. \tag{18b}$$

The functions $\Phi_e(j/Kt)$ are shown in Fig. 8(b) and the functions $G(\Phi)$ for several k_BT/Kv in Fig. 10.

IV. EXPERIMENT

Polycrystalline $Ir_{22}Mn_{78}$ films of different thicknesses have been deposited at room temperature onto 16 nm thick ferromagnetic $Ni_{81}Fe_{19}$ films by sputtering in a 10 target UHV system at an Ar(6N) pressure of 5×10^{-3} mbar with an in plane magnetic field of 4 kA/m. This field generates a deposition induced uniaxial anisotropy of about 10^2 J/m^3 in the Ni-Fe film. We used oxidized Si wafer substrates with a 4 nm thick Ta buffer layer. We also deposited a 4 nm Ta cap layer for final protection. The buffer layer induces a strong (111) texture of the NiFe/IrMn system with a FWHM of the rocking curve of $\Delta\Theta_{50}\approx6^\circ$, columnar growth and a grain size of 15 ± 3 nm as determined by AFM and SEM. The specimen size was $S=7\times6$ mm^2.

A nominal film thickness t_{nom} was determined from the deposition time and rate, which was controlled by AFM, RBS, and a stylos-based surface profiler for thicker films. Film thicknesses below 2 nm have to be controlled very carefully because the film properties near both interfaces (NiFe/IrMn and IrMn/cap layer) can be different from those in the volume between them. Therefore, we investigated separately the film thickness dependence of the rotational loss E_L in the equilibrium state of field rotation at $T=10$ K for film systems with different cap layer metals (Ta, Ru, Cu) and with different ferromagnetic layers (NiFe, CoFe, CoFe+0.6 nm Cu). As a result of these experiments we found:[20]

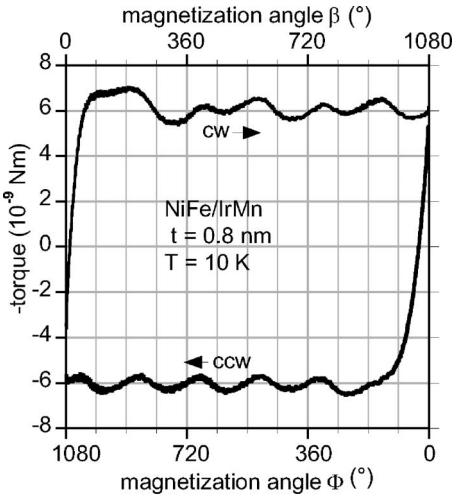

FIG. 12. Torque as a function of the field angle before (cw) and after (ccw) rotation reversal, as measured for a NiFe(16 nm)/IrMn(0.8 nm) film.

(1) For Ta/NiFe/IrMn(t)/cap layer the function $E_L(t)$ is always the same as shown in Fig. 11 if the nominal IrMn film thickness is reduced to $t=t_{nom}-\Delta t$ with $\Delta t\pm0.1$ nm $=0.7$ nm, 0.2 nm, 0 nm for cap layers of Ta, Ru, Cu, respectively.

(2) $E_L(t)$ is also the same curve as shown in Fig. 11 for different ferromagnetic layers if the thickness is corrected only with respect to the cap layer metal and if $t<1$ nm, (for $t>1$ nm E_L depends on the ferromagnetic film).

(3) A "dead" layer with a thickness Δt is most likely caused by resputtering from the IrMn film by energetic particles in the sputtering gas during the initial part of the cap layer deposition.

It is well known that highly energetic particles originate from positive ions (Ar^+) accelerated to the sputtering cathode which are then reflected after electrical neutralization. The energy of these reflected particles and, thus, the resputtering rate, increases strongly for higher ratios of the target atomic mass to the Ar mass which is 181/40, 101/40, 64/40 for a target of Ta, Ru, Cu, respectively. In this paper we used only Ta cap layers. Therefore, we take $t=t_{nom}-0.7$ nm without further corrections. Figure 11 shows that at $T=10$ K the loss is large in the region $t=(0.8$ to $1.5)$ nm which, therefore, was selected also for the present study of the nonequilibrium rotational losses. Our films of $t\geqslant0.7$ nm have a continuous structure. This is concluded from previous investigations of NiFe/IrMn(t)/AAF film systems which had been prepared in the same way as the NiFe/IrMn(t) films in this paper but completed by an additional artificial antiferromagnet film AAF on top of the IrMn(t).[11] Pinholes in these IrMn films cause exchange interaction between the NiFe and the AAF. This has been measured for films thinner than 0.7 nm but for $t\geqslant0.7$ nm pinholes have not been found.

Torque measurements were carried out with a home-made torque meter described previously[21] in the temperature range $T=(10$ to $300)$ K, with a magnetic field of $\mu_0H=0.6$ Tesla rotating at $\pm180^\circ$/min in the film plane and with torque measurement every 0.5°.

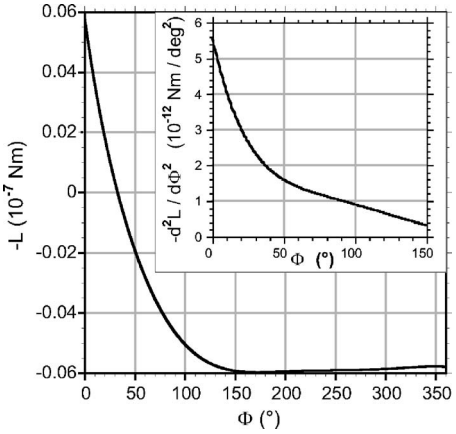

FIG. 13. Torque $L(\Phi)$ after rotation reversal as a function of the magnetization angle Φ. Data from Fig. 12. Inset: Second derivative of $L(\Phi)$.

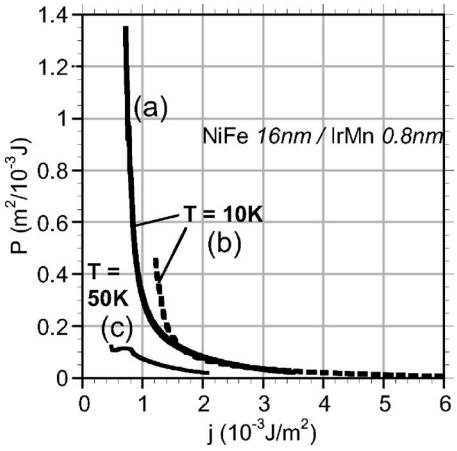

FIG. 14. Coupling strength distribution $P(j)$ as a function of the coupling energy density j of a film system NiFe(16 nm)/IrMn(0.8 nm) as determined with Eq. (17a) from torque measurements at $T=10$ K (a) and (b), and at $T=50$ K (c). The AF anisotropy constant K was used as a variable parameter: $K=3.5\times10^5$ J/m^3 for (a) and (c), and $K=5.6\times10^5$ J/m^3 for (b), corresponding to a thermal activation of $k_BT/Kv=0.0029$ (a), 0.0018 (b), and 0.0143 (c), respectively.

For our measurements at low temperature the films were cooled down with H rotating in order to minimize any frozen integral unidirectional exchange bias anisotropy. Only the torque of interest from losses in the F/AF system depends on the rotational direction. The torque contribution L_F of the anisotropy of the F film can be easily separated because it is the same for cw and ccw rotation and it is independent of the number of full rotations. $L_F(\Phi)-L_F(\Phi+720°)=0$. Figure 12 shows the original measured torque curve of a film system, with $t=0.8$ nm at $T=10$ K, as a function of magnetization angle β for 3 turns cw ($\beta=0$ to 1080°) followed by three turns ccw after a prompt rotation reversal. As can be seen, unidirectional anisotropy and, therefore, also exchange bias is negligible while the rotational loss is large as expected from Fig. 11.

Exchange bias for this film system was measured only after field cooling in a nonrotating field: $H_{EB}(10\text{ K})=16$ Oe is estimated from $H_{EB}=J/M_Ft_F$, with a measured unidirectional coupling energy density of $J(10\text{ K})=20\ \mu$J/m^2 induced by this field cooling. ($J=A_1/S$ is determined from the Fourier component A_1 of the torque curve $L=A_0+A_1\sin\beta+\cdots$). At room temperature $H_{EB}=0$ and $H_C=1.6$ Oe, as determined by MOKE measurements from the rectangular hysteresis loop, thereby indicating a high quality of the film system. H_C at low temperatures has not been measured.

The magnetization angle β only slightly deviates from the field angle β_H, which was considered in the experiments. ($\beta=\beta_H-\varepsilon$ with $\varepsilon=\arcsin[-L(\beta_H)/HM_FV_F]\leqslant1.3°$; V_F is the volume of the F film). We evaluate the difference curve $\Delta L(\Phi)=L_{ccw}(\Phi)-L_{ccw}(\Phi+720°)$ which eliminates the contribution of the uniaxial anisotropy of the F film and is independent of the reversal position $\Phi=0$ on the cw torque curve. For the analysis of the coupling strength distribution $P(j)$ we take $L(\Phi)=\Delta L(\Phi)-0.5\Delta L(0)$ which is shifted with respect to $\Delta L(\Phi)$ by half its maximum value. Thus, $L(\Phi)$ is consistent with Eq. (10). Figure 13 shows $L(\Phi)$ derived from Fig. 12 and $d^2L/d\Phi^2$ versus Φ in the inset. The ccw equilibrium state is achieved near $\Phi=150°$ which is the angle calculated for film crystallites with a 3-axial symmetry ($q=3$). Taking K as a parameter we calculated the distribution function $P(j)$ from $d^2L/d\Phi^2$ by using the Eqs. (17a), (18a), and (18b).

V. RESULTS AND DISCUSSION

Figure 14 shows distribution functions $P(j)$ as determined for a film system with $t=0.8$ nm which was measured at two different temperatures T. The measurement at $T=10$ K is evaluated with the anisotropy $K=3.5\times10^5$ J/m^3 (curve a) and with $K=5.6\times10^5$ J/m^3 (curve b). For comparison, the measurement at $T=50$ K is also evaluated with $K=3.5\times10^5$ J/m^3 (curve c). As can be seen from curves a and b the final results are rather sensitive to the anisotropy K. K is not known exactly but it is expected to be $(3\pm1)\times10^5$ J/m^3 from our separate investigations[22] and from the uniaxial anisotropy $K_u^{\text{eff}}=2\times10^5$ J/m^3 of thicker IrMn films estimated by Carey *et al.*[23] Even without knowledge of the exact K value the analysis of our experiments with $K=(2\text{ to }4)\times10^5$ J/m^3 confirm that

(1) P decreases with increasing j,

(2) most of the crystallites are weakly coupled with $j<1\times10^{-3}$ J/m^2,

(3) the portion of strongly coupled grains ($j>1\times10^{-3}$ J/m^2) reduces with increasing temperature from 20 to 30 % at $T=10$ K to about 5% at 50 K.

If K is set too small our measurements obviously yield incorrect $P(j)$ distributions because then $\int_0^\infty P(j)dj>1$, which is not possible. Furthermore, the torque measurements $L(\Phi)$ in the range $\Phi>120°$ systematically showed a curvature which seems to be something too large and not disappearing at $\Phi=150°$ (see Fig. 13) as expected from theory. Therefore, we applied only the range $\Phi=(0\text{ to }120)°$ for the evaluation of P in Fig. 14. We do not know the reason for this behavior. Possibly it is connected with some grain interaction[3] which is

TABLE I. Critical coupling densities j_1 and j_2, amount of grains contributing to rotational loss, total loss density E_L and a roughly estimated unidirectional coupling density J, corresponding to Fig. 14 for $K=3.5\times10^5$ J/m^3. Measured values of E_L and J are in the last three rows.

	$T=10$ K	$T=50$ K
j_1 (10^{-3} J/m^2)	0.75	0.46
j_2 (10^{-3} J/m^2)	3.5	2.1
$\int_0^{j_1}P(j)dj=1-\int_{j_1}^{\infty}P(j)dj$	0.60	0.88
$\int_{j_1}^{j_2}P(j)dj$	0.38	0.11
$\int_{j_2}^{\infty}P(j)dj$	~0.02	~0.01
$E_L=\int_{j_1}^{j_2}P(j)\Delta e(j)dj$ (10^{-3} J/m^2)	0.90	0.12
$J=P_0j_1^2/2$ (10^{-3} J/m^2)	0.22	0.20
$E_L=\frac{\pi}{S}\Delta L(\Phi=0)$ (10^{-3} J/m^2)	0.90	0.12
J (cooling for H rotating) (10^{-3} J/m^2)	0	0
J (cooling for H=constant) (10^{-3} J/m^2)	0.020	<0.020

not included in our model. An assumed grain interaction coupling would be relative more important in the region $\Phi=(120\text{ to }150)^\circ$ which is represented in our model by grains of small F/AF coupling j, than for grains of larger j represented by the lower angles Φ. Furthermore, we expect interactions for only a very small amount of grains which effectively have no grain boundary and minor lattice mismatch between them.

Table I shows for $K=3.5\times10^5$ J/m^3 in Fig. 14 the critical coupling densities j_1 and j_2, the percentages of grains with $j<j_1$, $j_1<j<j_2$, and $j>j_2$, the integrated loss density E_L, the unidirectional coupling energy density J as estimated from $P(j)$ and measured values of E_L and J. Only one percent of all grains are coupled so strongly that their spin system can be rotated across all in-plane anisotropy axes without rotational loss. The amount of grains contributing to rotational loss decreases from ~40% at $T=10$ K to ~10% at 50 K. Their loss density E_L, determined from integration of the function $P(j)$, is in accordance with the measured values.

Most of the grains are coupled weekly thus they do not contribute to the rotational loss. Their amount increases with T from ~60% at $T=10$ K to ~90% at 50 K, but their average coupling strength $0<j<j_1$ decrease with increasing T. All these grains, if completely oriented by field cooling, are expected to contribute to the unidirectional coupling J and to H_{EB}. However, the experimental J value ($20\ \mu$J/m^2) is smaller by a factor 10 than the roughly estimated values in the table. For this estimation a constant coupling density P_0 for all grains with $0<j<j_1$ and $P_0=(1-\int_{j_1}^{\infty}P(j)dj)/j_1$ has been used. Although J and the corresponding H_{EB} can be estimated only indirectly by the loss measurements the large discrepancy of these J values requires further investigation. Possible contributions to the reduced measured J values are an incomplete moment orientation during field cooling, and an out of plane rotation of some AF moments which is not included in our model.

The proposed method is best suited to low temperatures, where thermal activation is a minimum. For $k_BT/Kv<0.001$ (corresponding to $T<4$ K for the film used) the function $G(\Phi)$ is nearly independent of T (see Fig. 10). In this case the model for $T=0$ can be applied which allows in addition the determination of $P(j/Kt)$ for film systems with grains of different Kt as well as the determination of $P(j)$ for film systems with grains of equal Kt but with Kt as a variable parameter.

Compared with methods based on hysteresis cycle measurements such as bias field and coercivity evolution and relaxation, the proposed method has the advantage of directly measuring the energy loss independent of its complex influence on the coercivity. Furthermore, exchange bias depends on the degree of preferred AF moment orientation, for instance after a field cooling process, while losses are independent of this preferred orientation. As compared with measurements of a blocking temperature distribution the proposed method advantageously is applied at a constant temperature T, thus, giving the coupling strength distribution just for this T. Therefore the method is independent of possible temperature dependencies of K and of $P(j)$.

VI. CONCLUSIONS

The proposed measuring method was shown to be suited to the determination of the coupling strength distribution $P(j)$ for F/AF film systems with small thickness t and known values of anisotropy constant and film thickness. It takes advantage of the high magnetic field applied which enables magnetic saturation of the F film and of the high sensitivity of torquemetry. A torquemeter with control of low temperatures and with high angular resolution is required because the second derivative of a torque curve after field rotation reversal must be carefully evaluated. Further experiments are desirable with well defined film systems of larger grain size and at lower temperatures (less thermal relaxation, and less grain interaction) in order to check and improve this new method. With respect to the simplified model used and its plausible but not proven assumptions the agreement between calculations and experiments is good. The model calculations with thermal activation can also be applied to estimating the T-dependence of losses in F/AF films, and their blocking temperature and AF anisotropy constant.

ACKNOWLEDGMENTS

The authors would like to thank M. Diegel and Th. Klupsch for fruitful discussions, W. Michalke and K. Kirsch for film depositions, and S. Schmidt for experimental assistance.

[1] W. H. Meiklejohn and C. P. Bean, Phys. Rev. **102**, 1413 (1956); Phys. Rev. **105**, 904 (1957).
[2] E. Fulcomer and S. H. Charap, J. Appl. Phys. **43**, 4190 (1972).
[3] H. Fujiwara, J. Magn. Soc. Jpn. **26**(12), 1151 (2002).
[4] M. Ali, C. H. Marrows, M. Al-Jawad, B. J. Hickey, A. Misra, U. Nowak, and K. D. Usadel, Phys. Rev. B **68**, 214420 (2003).
[5] M. Tsunoda and M. Takahashi, J. Magn. Magn. Mater. **239**, 149 (2002).
[6] M. Takahashi and M. Tsunoda, J. Phys. D **35**, 2365 (2002).
[7] J. Nogués and I. K. Schuller, J. Magn. Magn. Mater. **192**, 203 (1999).
[8] A. E. Berkowitz and K. Takano, J. Magn. Magn. Mater. **200**, 552 (1999).
[9] D. Hrabovský, B. Diouf, L. Gabillet, A. Audouard, A. R. Fert, and J. F. Bobo, Eur. Phys. J. B **45**, 273 (2005).
[10] D. Venus, F. Hunte, I. N. Krivorotov, T. Gredig, and E. Dan Dahlberg, J. Appl. Phys. **93**, 8609 (2005).
[11] R. Mattheis and K. Steenbeck, J. Appl. Phys. **97**, 10K107 (2005).
[12] K. Steenbeck, R. Mattheis, and M. Diegel, J. Magn. Magn. Mater. **279**, 317 (2004).
[13] M. Ali, C. H. Marrows, and B. J. Hickey, Phys. Rev. B **67**, 172405 (2003).
[14] K. Takano, R. H. Kodama, A. E. Berkowitz, W. Cao, and G. Thomas, J. Appl. Phys. **83**, 6888 (1998).
[15] M. D. Stiles and R. D. McMichael, Phys. Rev. B **60**, 12950 (1999).
[16] V. Baltz, J. Sort, B. Rodmacq, B. Dieny, and S. Landis, Appl. Phys. Lett. **84**, 4923 (2004).
[17] S. Soeya, T. Imagawa, K. Mitsuoka, and S. Narishige, J. Appl. Phys. **76**, 5356 (1994).
[18] G. W. Anderson, Y. Huai, and M. Pakala, J. Appl. Phys. **87**, 5726 (2000).
[19] S. A. Araki, M. Sano, M. Ohta, Y. Tsuchiya, K. Noguchi, H. Morita, and M. Matsuzaki, IEEE Trans. Magn. **34**, 1426 (1998).
[20] K. Steenbeck and R. Mattheis (unpublished).
[21] R. Hergt, W. Andrä, K. Fischer, N. M. Chebotayev, and S. L. Town, Phys. Status Solidi A **119**, 241 (1990).
[22] K. Steenbeck, R. Mattheis, and M. Diegel, J. Appl. Phys. (to be published).
[23] M. J. Carey, N. Smith, B. A. Gurney, J. R. Childress, and T. Lin, J. Appl. Phys. **89**, 6579 (2001).